Journal of Organometallic Chemistry, 353 (1988) 343–353
Elsevier Sequoia S.A., Lausanne – Printed in The Netherlands

Structural studies on ruthenium carbonyl hydrides

XIV *. Synthesis, characterization, and crystal structure of $(\mu\text{-H})_2Ru_3(\mu_3\text{-}\eta^2\text{-CHC(O)OCH}_3)(CO)_8(PPh_3)$. An example of *cis*-labilization by an oxygen donor ligand

Thomas S. Janik **

Department of Chemistry, State University College at Fredonia, State University of New York, Fredonia, New York 14063 (U.S.A.)

Melvyn Rowen Churchill, Timothy P. Duggan, and Jerome B. Keister

Department of Chemistry, University at Buffalo, State University of New York, Buffalo, New York 14214 (U.S.A.)

(Received April 5th, 1988)

Abstract

The reaction of PPh_3 with $(\mu\text{-H})_2Ru_3(\mu_3\text{-}\eta^2\text{-CHC(O)OCH}_3)(CO)_9$ displaces a CO ligand, rather than the coordinated oxygen atom of the acyl moiety, thereby generating $(\mu\text{-H})_2Ru_3(\mu_3\text{-}\eta^2\text{-CHC(O)OCH}_3)(CO)_8(PPh_3)$. A single-crystal X-ray study of $(\mu\text{-H})_2Ru_3(\mu_3\text{-}\eta^2\text{-CHC(O)OCH}_3)(CO)_8(PPh_3)$ has been performed. This complex crystallizes in the triclinic space group $P\bar{1}$ with a 9.360(1), b 11.442(1), c 15.192(1) Å, α 84.554(7), β 78.729(8), γ 83.023(3)°, V 1579.6(3) Å^3 and $Z = 2$. Data for 2θ 5.0–50.0° (Mo-K_α) were collected on a Syntex $P2_1$ automated four-circle diffractometer and the structure was refined to R_F 4.6% for all 5601 reflections (R_F 3.4% for those 4962 reflections with $|F_o| > 3\sigma(|F_o|)$). The crystal structure establishes that PPh_3 substitution occurs *cis* to the coordinated oxygen in that equatorial site which is *trans* to the non-hydrido-bridged Ru–Ru bond. The high rate of CO displacement from $(\mu\text{-H})_2Ru_3(\mu_3\text{-}\eta^2\text{-CHC(O)OCH}_3)(CO)_9$, as compared with that for $(\mu\text{-H})_3Ru_3(\mu_3\text{-CC(O)OCH}_3)(CO)_9$, is attributed to *cis* labilization by the oxygen donor atom.

---

* For previous parts see refs. 1–4.

** Address correspondence to this author.

0022-328X/88/$03.50

Introduction

In previous work we showed that $(\mu\text{-H})_2Ru_3(\mu_3\text{-}\eta^2\text{-CHC(O)OCH}_3)(CO)_9$ is a possible intermediate in the reductive elimination of methyl acetate from $(\mu\text{-H})_3Ru_3(\mu_3\text{-CC(O)OCH}_3)(CO)_9$ [2,5]. The alkylidene ligand is stabilized by coordination of the oxygen atom of the acyl to one of the ruthenium atoms. In an attempt to synthesize an alkyl intermediate, we reacted $(\mu\text{-H})_2Ru_3(\mu_3\text{-}\eta^2\text{-CHC(O)OCH}_3)(CO)_9$ with PPh_3, hoping to displace the stabilizing acyl. Instead, $(\mu\text{-H})_2Ru_3(\mu_3\text{-}\eta^2\text{-CHC(O)OCH}_3)(CO)_9$ was found to be very labile toward CO replacement. The product from the reaction has been characterized by spectroscopic methods and by a single-crystal X-ray structural determination as $(\mu\text{-H})_2Ru_3(\mu_3\text{-}\eta^2\text{-CHC(O)OCH}_3)(CO)_8(PPh_3)$, the formation of which involves displacement of a CO ligand *cis* to the oxygen donor atom.

Experimental

General

$(\mu\text{-H})_3Ru_3(\mu_3\text{-CC(O)OCH}_3)(CO)_9$ [6] and $(\mu\text{-H})_2Ru_3(\mu_3\text{-}\eta^2\text{-CHC(O)OCH}_3)(CO)_9$ [2] were prepared according to previously published procedures. Infrared spectra were recorded with a Beckman 4250 spectrophotometer; solutions in cyclohexane were used and the 2138.5 cm^{-1} absorption of cyclohexane was used as reference. ^1H NMR spectra were recorded with a JEOL FX-90Q spectrometer. Mass spectra were obtained with a VG 70SE mass spectrometer. Elemental analyses were performed by Schwarzkopf Microanalytical Laboratories.

$(\mu\text{-H})_2Ru_3(\mu_3\text{-}\eta^2\text{-CHC(O)OCH}_3)(CO)_8(PPh_3)$

In a 50 ml Schlenk flask equipped with reflux condenser, stir bar, and nitrogen gas inlet were placed $(\mu\text{-H})_3Ru_3(\mu_3\text{-CC(O)OCH}_3)(CO)_9$ (48 mg, 0.076 mmol) and heptane (25 ml). The solution was heated at 89–90 °C for 2 h, until the IR spectrum indicated complete conversion of starting material to $(\mu\text{-H})_2Ru_3(\mu_3\text{-}\eta^2\text{-CHC(O)OCH}_3)(CO)_9$. Then PPh_3 (30 mg, 0.11 mmol) was added to the solution at 25 °C, causing an immediate color change from yellow to red-orange. The heptane was removed by the use of a rotary evaporator. The residue was separated by using thin layer chromatography on silica and eluting with dichloromethane/hexanes (1/5 v/v). Extraction of the second, dark orange band with dichloromethane and evaporation yielded $(\mu\text{-H})_2Ru_3(\mu_3\text{-}\eta^2\text{-CHC(O)OCH}_3)(CO)_8(PPh_3)$ (22 mg, 34%). The product was recrystallized from methanol to obtain analytically pure material and for X-ray quality crystals.

IR (C_6H_{12}): 2093s, 2055vs, 2028s, 2020s, 2008m, 1989s, 1977m, 1955m, and 1538vw cm^{-1}. ^1H NMR ($CDCl_3$, 22 °C): 7.4 (m, 15H, PPh_3), 3.94 (s, 1H, $CHCO_2CH_3$), 3.20 (s, 3H, CH_3), −12.7 (br, 1H, Ru–H–Ru), and −14.4 (br, 1H, Ru–H–Ru) ppm; (−20 °C): 7.4 (m, 15H), 3.94 (s, 1H), 3.20 (s, 3H), −12.7 (dd, $1H_a$), and −14.4 (dd, $1H_b$) ppm, J_{ab} 2.9, J_{aP} 3.7, and J_{bP} 10.3 Hz. MS (EI): m/z 872 ($^{104}Ru_3$). Anal. Found: C, 40.06; H, 2.49. $C_{29}H_{21}O_{10}PRu_3$ calc: C, 40.33; H, 2.45%.

Collection of the X-ray diffraction data

The crystal chosen for the diffraction study was a well-formed, orange-red parallelepiped of approximate orthogonal dimensions $0.2 \times 0.2 \times 0.4$ mm^3. The

Table 1

Experimental data for the X-ray diffraction study of $(\mu\text{-H})_2Ru_3(\mu_3\text{-}\eta^2\text{-CHC(O)OCH}_3)(CO)_8(PPh_3)$

(A) Unit cell data			
a	9.360(1) Å	crystal system: triclinic	
b	11.442(1) Å	space group: $P\bar{1}$	
c	15.192(1) Å	$Z = 2$	
α	84.554(7)°	formula: $C_{29}H_{21}O_{10}PRu_3$	
β	78.729(8)°	mol. mass = 863.5 amu	
γ	83.023(3)°	D_{calc} 1.81 g/cm^3	
V	1579.6(3) Å^3	T 297 K	

(B) Collection of X-ray diffraction data

Diffractometer:	Syntex $P2_1$
Radiation:	Mo-K_α ($\bar{\lambda}$ 0.710730 Å)
Monochromator:	Highly oriented (pyrolytic) graphite; equatorial mode with $2\theta(m) = 12.160°$; assumed to be 50% perfect, 50% ideally mosaic for polarization correction.
Reflections meas'd:	$+h, \pm k, \pm l$ for $2\theta = 5.0° \rightarrow 50.0°$, yielding 5601 unique data.
Scan type:	Coupled θ(crystal)–2θ(counter)
Scan width:	$[2\theta(K_{\alpha_1}) - 0.9]° \rightarrow [2\theta(K_{\alpha_2}) + 0.9]°$
Scan speed:	4.0 deg/min (2θ)
Backgrounds:	Stationary-crystal, stationary-counter at the two extremes of the 2θ scan; each for one quarter of the total scan time.
Standard reflections:	Three approximately mutually orthogonal reflections collected before each set of 97 data points. No significant fluctuations nor decay were observed.
Absorption correction:	μ(Mo-K_α) = 14.9 cm^{-1}; corrected empirically by interpolation (in 2θ and ϕ) for 9 close-to-axial (ψ-scan) reflections.

crystal was mounted along its extended axis in a thin-walled capillary and was aligned and centered on a Syntex $P2_1$ automated four-circle diffractometer. Determination of accurate cell dimensions and the crystal's orientation matrix were performed as described previously [7]. Details of this and the data collection are provided in Table 1.

Examination of the data set revealed no systematic absences and no symmetry other than the Friedel condition ($\bar{1}$). Thus the crystal belongs to the triclinic class with space group $P1$ or $P\bar{1}$. The latter, centrosymmetric possibility was strongly indicated by the cell volume (consistent with $Z = 2$) and was confirmed by the successful solution of the structure in this higher symmetry space group. Data were corrected for absorption (by interpolation in ϕ and 2θ between a set of normalized transmission curves based upon ψ-scans of close-to-axial reflections) and for Lorentz and polarization effects. All data were converted to unscaled $|F_o|$ values; any reflection with $I < 0$ was assigned the value $|F_o| = 0$; symmetry-equivalent data were averaged and the resulting unique data set was placed on an approximately absolute scale by use of a Wilson plot (overall isotropic thermal parameter, $\bar{B}$ 2.71 Å^2).

Solution and refinement of the structure

All subsequent calculations were performed on the SUNY-Buffalo modified version of the Syntex XTL interactive crystallographic program package [8]. The locations of the three ruthenium atoms were determined by use of a Patterson map.

Table 2

Final atomic positional parameters for $(\mu\text{-H})_2Ru_3(\mu_3\text{-}\eta^2\text{-CHC(O)OCH}_3)(CO)_8(PPh_3)$ [a]

(A) Positional and isotropic thermal parameters

Atom	x	y	z	B (Å^2)
Ru(1)	0.09335(4)	0.23741(3)	0.23510(2)	
Ru(2)	−0.00961(4)	0.23439(4)	0.07622(2)	
Ru(3)	0.27421(4)	0.30145(4)	0.05546(2)	
P(1)	0.22402(13)	0.22755(11)	0.35671(8)	
O(1)	0.19423(36)	0.06374(27)	0.20636(21)	
O(2)	0.29354(40)	−0.05797(30)	0.09990(23)	
O(11)	−0.17785(48)	0.14118(44)	0.34778(31)	
O(12)	−0.04814(48)	0.48650(35)	0.24829(30)	
O(21)	−0.04134(56)	0.23630(46)	−0.12078(29)	
O(22)	−0.15892(52)	0.01543(40)	0.14781(31)	
O(23)	−0.28331(51)	0.40624(43)	0.13116(32)	
O(31)	0.33536(59)	0.55586(40)	0.07430(31)	
O(32)	0.57694(49)	0.18251(49)	0.07392(35)	
O(33)	0.32240(53)	0.31126(44)	−0.14907(26)	
C(1)	0.19875(53)	0.13179(43)	0.05241(32)	
C(2)	0.22782(49)	0.04713(41)	0.12437(32)	
C(3)	0.32514(79)	−0.14432(53)	0.17027(43)	
C(11)	−0.07684(60)	0.17737(48)	0.30428(35)	
C(12)	0.00601(56)	0.39121(49)	0.24516(33)	
C(21)	−0.03106(60)	0.23565(49)	−0.04808(39)	
C(22)	−0.10492(59)	0.09909(51)	0.12124(36)	
C(23)	−0.18127(62)	0.34391(51)	0.11098(36)	
C(31)	0.31086(64)	0.46347(54)	0.06626(36)	
C(32)	0.46651(61)	0.22871(55)	0.06515(37)	
C(33)	0.30706(68)	0.31137(51)	−0.07399(37)	
C(41)	0.11255(52)	0.24992(43)	0.46925(32)	3.184(86)
C(42)	−0.00962(58)	0.33511(46)	0.47521(35)	3.79(10)
C(43)	−0.09020(65)	0.36726(52)	0.55930(40)	4.60(12)
C(44)	−0.04747(72)	0.31165(57)	0.63911(44)	5.25(13)
C(45)	0.07371(81)	0.22211(64)	0.63218(49)	6.23(15)
C(46)	0.15345(73)	0.19315(59)	0.54811(45)	5.44(13)
C(51)	0.32855(52)	0.08345(42)	0.36761(32)	3.060(85)
C(52)	0.47268(56)	0.06532(46)	0.32701(34)	3.59(10)
C(53)	0.55049(68)	−0.04925(55)	0.33049(41)	4.88(12)
C(54)	0.47935(68)	−0.14066(54)	0.37295(41)	4.91(12)
C(55)	0.33618(71)	−0.12443(57)	0.41364(43)	5.17(13)
C(56)	0.25750(62)	−0.01426(51)	0.41183(38)	4.30(11)
C(61)	0.35882(51)	0.33249(41)	0.35321(31)	2.981(84)
C(62)	0.35441(56)	0.43568(45)	0.29799(34)	3.523(94)
C(63)	0.45128(64)	0.51846(51)	0.29732(39)	4.47(11)
C(64)	0.55523(69)	0.49885(56)	0.35009(42)	4.99(12)
C(65)	0.56075(73)	0.39529(59)	0.40666(44)	5.45(14)
C(66)	0.46363(65)	0.31353(53)	0.40847(40)	4.57(12)
H(1)	0.2334(48)	0.1035(38)	−0.0084(31)	2.7(10)
H(13)	0.2510(58)	0.2780(47)	0.1676(35)	4.9(13)
H(23)	0.0988(61)	0.3624(49)	0.0615(37)	5.6(14)
H(31)	0.3507	−0.2222	0.1522	3.0
H(32)	0.2301	−0.1476	0.2156	3.0
H(33)	0.3916	−0.1197	0.2000	3.0
H(42)	0.0931	0.3240	0.4781	3.0
H(43)	−0.0417	0.3001	0.5890	3.0
H(44)	−0.1077	0.2522	0.6715	3.0

Table 2 (continued)

(A) Positional and isotropic thermal parameters

Atom	x	y	z	B (Å^2)
H(45)	−0.0121	0.2103	0.6798	3.0
H(46)	0.1394	0.1334	0.5077	3.0
H(52)	0.5379	0.0596	0.2692	3.0
H(53)	0.5829	−0.0081	0.2718	3.0
H(54)	0.5328	−0.2190	0.3764	3.0
H(55)	0.2881	−0.1910	0.4450	3.0
H(56)	0.1823	0.0386	0.3880	3.0
H(62)	0.2827	0.4500	0.2587	3.0
H(63)	0.4451	0.5917	0.2586	3.0
H(64)	0.6266	0.5545	0.3465	3.0
H(65)	0.6340	0.3833	0.4451	3.0
H(66)	0.4683	0.2424	0.4484	3.0

(B) Anisotropic thermal parameters

Atom	B_{11}	B_{22}	B_{33}	B_{12}	B_{13}	B_{23}
Ru(1)	2.487(16)	2.753(17)	2.158(15)	−0.072(12)	−0.473(12)	−0.407(12)
Ru(2)	2.749(17)	3.331(18)	2.566(17)	−0.151(13)	−0.945(13)	−0.292(13)
Ru(3)	2.878(17)	3.509(19)	2.407(17)	−0.591(14)	−0.302(13)	−0.066(13)
P(1)	2.756(51)	3.132(54)	2.140(46)	−0.299(41)	−0.518(39)	−0.145(39)
O(1)	3.72(15)	2.97(14)	2.63(14)	0.27(12)	−0.75(12)	−0.35(11)
O(2)	4.63(18)	3.41(16)	3.88(17)	1.08(14)	−1.02(14)	−1.26(13)
O(11)	4.39(21)	8.33(30)	6.12(25)	−2.88(20)	0.97(19)	−0.42(21)
O(12)	6.32(24)	3.75(20)	6.68(25)	1.50(17)	−2.50(20)	−1.93(17)
O(21)	8.31(30)	9.00(32)	3.41(19)	−0.92(24)	−2.68(20)	−0.60(19)
O(22)	6.72(26)	5.12(23)	6.56(26)	−2.39(20)	−1.07(21)	−0.08(19)
O(23)	5.29(23)	7.00(27)	6.58(26)	1.96(21)	−1.33(20)	−1.96(21)
O(31)	9.50(33)	4.50(22)	6.06(25)	−2.80(22)	−1.59(23)	−0.04(19)
O(32)	3.72(21)	9.81(35)	8.08(30)	1.00(22)	−1.89(20)	−2.37(25)
O(33)	7.70(28)	7.99(29)	2.59(18)	−1.50(22)	−0.18(17)	0.09(17)
C(1)	3.36(22)	3.48(23)	2.40(20)	−0.27(18)	−0.61(17)	−0.63(17)
C(2)	2.37(19)	3.01(21)	3.35(22)	−0.00(16)	−0.69(16)	−0.54(17)
C(3)	7.79(40)	3.85(28)	4.99(32)	1.30(27)	−2.56(29)	−0.88(24)
C(11)	3.67(24)	4.17(26)	3.38(23)	−0.35(20)	−0.46(20)	−0.93(19)
C(12)	3.51(23)	4.05(26)	3.20(22)	−0.12(20)	−1.19(18)	−0.87(19)
C(21)	3.89(25)	4.36(27)	4.19(28)	0.05(21)	−1.49(21)	−0.50(21)
C(22)	3.71(24)	4.12(27)	3.90(25)	−0.76(21)	−0.90(20)	−0.53(21)
C(23)	3.89(26)	4.67(28)	3.56(24)	0.13(22)	−1.30(28)	−0.61(21)
C(31)	4.70(28)	4.53(29)	3.23(24)	−1.18(23)	−0.54(20)	0.52(21)
C(32)	3.19(25)	5.82(32)	3.87(26)	−0.71(23)	−0.34(20)	−0.88(23)
C(33)	4.02(26)	4.75(28)	3.11(24)	−0.98(21)	−0.42(19)	0.37(20)

[a] The anisotropic thermal parameters are in standard XTL format and enter the expression for the calculated structure factor in the form: $\exp[-0.25(h^2a^{*2}B_{11} + k^2b^{*2}B_{22} + l^2c^{*2}B_{33} + 2hka^*b^*B_{12} + 2hla^*c^*B_{13} + 2klb^*c^*B_{23})]$.

Positions of all remaining atoms (excluding the phenyl hydrogens) were determined by subsequent difference-Fourier maps. The phenyl and methyl hydrogens were placed in idealized locations with d(C–H) 0.95 Å [9]. Positions of these hydrogen atoms were updated but were not refined during least-squares refinement of the structure. The function minimized during least-squares refinement is $\Sigma w(|F_o| - |F_c|)^2$, where $1/w = [\sigma(|F_o|)]^2 + [0.01|F_o|]^2$. Throughout the analysis, the analyti-

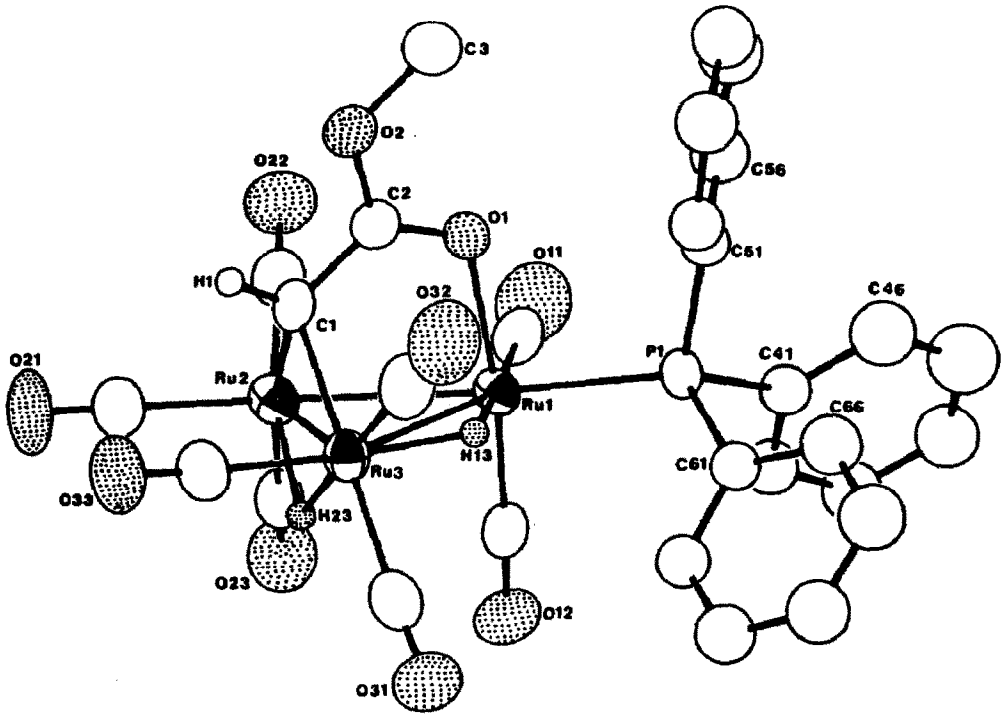

Fig. 1. Labeling of atoms in the $(\mu\text{-H})_2Ru_3(\mu_3\text{-}\eta^2\text{-CHC(O)OCH}_3)(CO)_8(PPh_3)$ molecule (ORTEP-II diagram [24]; 30% probability ellipsoids).

cal form of the scattering factor [10a] for the appropriate neutral atom used in calculating F_c was corrected for both real ($\Delta f'$) and imaginary ($\Delta f''$) components of anomalous dispersion [10b]. Refinement led to convergence [11*] with $R_F = 4.6\%$, $R_{wF} = 4.6\%$ and $GOF = 1.78$ for all 5601 unique data ($R_F = 3.4\%$ and $R_{wF} = 3.7\%$ for those 4962 data with $|F_o| > 3\sigma(|F_o|)$). A final difference-Fourier map showed no unexpected features (highest peak of 1 $e^-/\text{Å}^3$, near the position of a ruthenium atom); the structure is thus both correct and complete. Final atomic positional parameters are collected in Table 2. The labeling scheme is illustrated by Fig. 1.

Results and discussion

Addition of one equiv of PPh_3 to $(\mu\text{-H})_2Ru_3(\mu_3\text{-}\eta^2\text{-CHC(O)OCH}_3)(CO)_9$ results in rapid gas evolution. Substitution of PPh_3 for CO, forming $(\mu\text{-H}_2)Ru_3(\mu_3\text{-}\eta^2\text{-CHC(O)OCH}_3)(CO)_8(PPh_3)$, is complete within minutes. $(\mu\text{-H})_2Ru_3(\mu_3\text{-}\eta^2\text{-CHC(O)OCH}_3)(CO)_8(PPh_3)$ has been characterized by spectroscopy and by X-ray crystallography. The spectroscopic data for the complex in solution are fully consistent with the solid state structure (Fig. 1, vide supra). The IR spectrum contains only terminal CO absorptions and a weak band at 1538 cm^{-1} due to the coordinated acyl group (cf. 1540 cm^{-1} for $(\mu\text{-H})_2Ru_3(\mu_3\text{-}\eta^2\text{-CHC(O)OCH}_3)(CO)_9$).

* Reference number with asterisk indicates a note in the list of references.

Table 3

Interatomic distances (Å) for $(\mu\text{-H})_2Ru_3(\mu_3\text{-}\eta^2\text{-CHC(O)OCH}_3)(CO)_8(PPh_3)$

(a) Ru–Ru and Ru–H distances			
Ru(1)–Ru(2)	2.773(1)	Ru(2)–H(23)	1.85(6)
Ru(1)–Ru(3)	2.994(1)	Ru(3)–H(23)	1.69(6)
Ru(3)–Ru(2)	2.805(1)	Ru(3)–H(13)	1.68(5)
Ru(1)–H(13)	1.71(5)		
(B) Distances involving the μ_3-η^2-CHC(O)OCH$_3$ ligand			
Ru(2)–C(1)	2.136(5)	Ru(3)–C(1)	2.152(5)
Ru(1)–O(1)	2.140(3)	C(1)–H(1)	0.99(5)
C(1)–C(2)	1.435(7)	C(2)–O(1)	1.251(6)
C(2)–O(2)	1.334(6)	O(2)–C(3)	1.435(7)
(C) Ru–CO bond lengths			
Ru(1)–C(11)	1.894(6)	Ru(1)–C(12)	1.855(6)
Ru(2)–C(21)	1.936(6)	Ru(2)–C(22)	1.886(6)
Ru(2)–C(23)	1.933(6)	Ru(3)–C(31)	1.953(6)
Ru(3)–C(32)	1.916(6)	Ru(3)–C(33)	1.925(5)
(D) C–O distances			
C(11)–O(11)	1.141(7)	C(12)–O(12)	1.146(7)
C(21)–O(21)	1.127(7)	C(22)–O(22)	1.140(7)
C(23)–O(23)	1.130(8)	C(31)–O(31)	1.131(8)
C(32)–O(32)	1.128(8)	C(33)–O(33)	1.121(7)
(E) Distances involving the triphenylphosphine ligand			
Ru(1)–P(1)	2.394(1)	P(1)–C(41)	1.843(5)
P(1)–C(51)	1.823(5)	P(1)–C(61)	1.835(5)
C(41)–C(42)	1.404(7)	C(42)–C(43)	1.408(8)
C(43)–C(44)	1.420(9)	C(44)–C(45)	1.428(10)
C(45)–C(46)	1.395(10)	C(46)–C(41)	1.405(8)
C(51)–C(52)	1.369(7)	C(52)–C(53)	1.422(8)
C(53)–C(54)	1.352(9)	C(54)–C(55)	1.360(9)
C(55)–C(56)	1.381(9)	C(56)–C(51)	1.417(8)
C(61)–C(62)	1.383(7)	C(62)–C(63)	1.387(8)
C(63)–C(64)	1.363(9)	C(64)–C(65)	1.398(9)
C(65)–C(66)	1.376(9)	C(66)–C(61)	1.396(8)

The ^{1}H NMR spectrum contains exchange-broadened hydride resonances, but at $-20\,^\circ$C the hydrides appear as doublets of doublets with each coupling to ^{31}P as well as the other hydride resonance. The higher field hydride resonance displays the larger coupling to ^{31}P, allowing its assignment to H(13) in Fig. 1; presumably the higher field hydride resonance in the spectrum of $(\mu\text{-H})_2Ru_3(\mu_3\text{-}\eta^2\text{-CHC(O)-OCH}_3)(CO)_9$ is due to the analogous hydride ligand.

The structure of $(\mu\text{-H})_2Ru_3(\mu_3\text{-}\eta^2\text{-CHC(O)OCH}_3)(CO)_8(PPh_3)$ was proven definitively by means of X-ray crystallography. The crystal consists of discrete molecular units of $(\mu\text{-H})_2Ru_3(\mu_3\text{-}\eta^2\text{-CHC(O)OCH}_3)(CO)_8(PPh_3)$, which are separated by normal Van der Waals' distances; there are no abnormally short intermolecular contacts. Each molecule is chiral, but the crystal contains an ordered racemic mixture of the two enantiomeric forms by virtue of the C_i ($\bar{1}$) symmetry of the array. Figure 1 shows the geometry of the molecule. Interatomic distances and angles are listed in Tables 3 and 4 respectively.

Table 4

Selected interatomic angles (°) for $(\mu\text{-H})_2Ru_3(\mu_3\text{-}\eta^2\text{-CHC(O)OCH}_3)(CO)_8(PPh_3)$

(A) Internal angles of the $(\mu\text{-H})_2Ru_3$ core			
Ru(1)–Ru(2)–Ru(3)	64.94(1)	Ru(1)–H(13)–Ru(3)	124.3(32)
Ru(3)–Ru(1)–Ru(2)	58.05(1)	Ru(2)–H(23)–Ru(3)	104.5(29)
Ru(1)–Ru(3)–Ru(2)	57.02(1)		
(B) Angles around the ruthenium atoms			
Ru(2)–Ru(1)–C(11)	92.00(17)	Ru(1)–Ru(2)–C(21)	165.74(17)
Ru(2)–Ru(1)–C(12)	88.79(16)	Ru(1)–Ru(2)–C(22)	91.01(17)
Ru(2)–Ru(1)–P(1)	169.67(3)	Ru(1)–Ru(2)–C(23)	94.93(17)
Ru(2)–Ru(1)–O(1)	84.83(9)	Ru(1)–Ru(2)–C(1)	76.15(13)
Ru(2)–Ru(1)–H(13)	85.5(18)	Ru(1)–Ru(2)–H(23)	74.8(18)
Ru(3)–Ru(2)–C(21)	101.11(17)	Ru(3)–Ru(2)–C(22)	136.71(17)
Ru(3)–Ru(2)–C(23)	121.65(17)	Ru(3)–Ru(2)–C(1)	49.40(13)
Ru(2)–Ru(3)–C(31)	122.37(17)	Ru(2)–Ru(3)–C(32)	138.05(18)
Ru(2)–Ru(3)–C(33)	94.28(17)	Ru(2)–Ru(3)–C(1)	48.89(13)
Ru(1)–Ru(3)–C(31)	102.90(17)	Ru(3)–Ru(1)–C(11)	149.80(17)
Ru(1)–Ru(3)–C(32)	103.49(18)	Ru(3)–Ru(1)–C(12)	91.87(16)
Ru(1)–Ru(3)–C(33)	151.00(17)	Ru(3)–Ru(1)–P(1)	113.44(3)
Ru(1)–Ru(3)–C(1)	71.05(13)	Ru(3)–Ru(1)–O(1)	82.42(9)
Ru(1)–Ru(3)–H(23)	69.4(19)	Ru(3)–Ru(1)–H(13)	27.5(18)
C(11)–Ru(1)–C(12)	91.11(23)	C(21)–Ru(2)–C(22)	98.15(24)
C(11)–Ru(1)–P(1)	95.89(17)	C(21)–Ru(2)–C(23)	95.23(24)
C(11)–Ru(1)–O(1)	91.87(19)	C(21)–Ru(2)–C(1)	92.62(22)
C(11)–Ru(1)–H(13)	174.1(18)	C(21)–Ru(2)–H(23)	96.8(18)
C(12)–Ru(1)–P(1)	97.70(17)	C(22)–Ru(2)–C(23)	94.44(24)
C(12)–Ru(1)–O(1)	173.04(19)	C(22)–Ru(2)–C(1)	91.55(22)
C(12)–Ru(1)–H(13)	94.2(18)	C(22)–Ru(2)–H(23)	164.8(18)
P(1)–Ru(1)–O(1)	88.25(9)	C(23)–Ru(2)–C(1)	169.35(22)
P(1)–Ru(1)–H(13)	86.0(18)	C(23)–Ru(2)–H(23)	87.2(18)
O(1)–Ru(1)–H(13)	82.6(18)	C(1)–Ru(2)–H(23)	84.8(18)
C(31)–Ru(3)–C(32)	96.91(25)	C(33)–Ru(3)–C(1)	87.20(21)
C(31)–Ru(3)–C(33)	96.09(24)	C(33)–Ru(3)–H(13)	174.1(19)
C(31)–Ru(3)–C(1)	171.03(22)	C(33)–Ru(3)–H(23)	91.7(19)
C(31)–Ru(3)–H(13)	89.1(19)	C(31)–Ru(3)–H(23)	83.3(19)
C(32)–Ru(3)–C(33)	95.65(24)	C(32)–Ru(3)–H(13)	81.0(19)

We previously reported the structure of the unsubstituted parent complex, $(\mu\text{-H})_2Ru_3(\mu_3\text{-}\eta^2\text{-CHC(O)OCH}_3)(CO)_9$, from which the present compound is derived [2]. It is, therefore, of interest to note any changes in bond lengths upon substitution. In the following discussion, bond lengths of equivalent bonds of the parent complex will be included in square brackets.

The complex is based on a triangular array of ruthenium atoms and the molecular geometry has changed little from the overall structure of the parent compound. The site of phosphine substitution is the acyl-coordinating ruthenium {Ru(1)}, with the phosphine assuming an equatorial position. The shortest Ru–Ru bond remains the unsupported metal–metal interaction, Ru(1)–Ru(2) 2.773(1) Å

[2.778(1) Å]. The μ-hydrido-μ-alkylidene bridged metal–metal bond is somewhat longer,Ru(2)–Ru(3) 2.805(1) Å [2.800(1) Å]. The longest Ru–Ru bond still occurs between the equatorially hydrido-bridged metals, Ru(1)–Ru(3) 2.994(1) Å [2.967(1) Å]. The μ_3-η^2-$CHC(O)OCH_3$ ligand remains essentially unperturbed over the triangular arrangement of metals. Carbon atom C(1) bridges Ru(2) and Ru(3) with Ru(2)–C(1) 2.136(5) Å [2.138(4) Å] and Ru(3)–C(1) 2.152(5) Å [2.143(4) Å]. The distance from C(1), the α-carbon atom of the alkylidene ligand, to C(2) is 1.435(7) Å [1.450(5) Å]. The formal carbon–oxygen double bond is C(2)–O(1) 1.251(6) Å [1.247(5) Å]. The C–OCH_3 bond, C(2)–O(2), is 1.334(6) Å [1.331(5) Å]. Surprisingly, the donor O:→Ru linkage appears unaffected by substitution, Ru(1)–O(1) 2.140(3) Å [2.134(3) Å].

The metal–phosphorus distance is typical for phosphine-substituted triruthenium clusters [12–14], Ru(1)–P(1) 2.394(1) Å. The Ru–CO bond lengths range from 1.855(6) to 1.953(6) Å [1.863(5)–1.972(5) Å]. The shortest Ru–CO linkage is, as for the parent complex, that for the carbonyl ligand *trans* to the coordinated oxygen of the ester functionality, Ru(1)–C(12) 1.855(6) Å [1.869(15) Å]. The carbon–oxygen bond of this carbonyl ligand is also unaffected by the substitution of the phosphine C(12)–O(12) 1.146(7) Å [1.148(7) Å]. The remaining equatorial CO shows changes as expected for increased electron density at the metal, with Ru(1)–C(11) 1.894(6) Å [1.921(5) Å] and C(11)–O(11) 1.141(7) Å [1.126(6) Å]. The longest Ru–CO bond in the parent complex belongs to that carbonyl ligand which is lost upon substitution; the longest metal–carbonyl linkage in the present complex corresponds to the second-longest in the parent compound and is the Ru–CO bond *trans* to the alkylidene carbon {C(1)} and *cis* to both hydride ligands Ru(3)–C(31) 1.953(6) Å [1.955(5) Å]. The other carbonyl ligand *trans* to C(1) (and *cis* to one hydride) has a slightly shorter metal–carbon distance Ru(2)–C(23) 1.933(6) Å [1.927(6) Å].

The hydride ligands were located and refined. The listed metal–hydride distances which range from 1.69(6) to 1.85(6) Å (av. 1.73 ± 0.08 Å [1.77 ± 0.11 Å] are of limited precision. However, the essential stereochemical positions are precisely equivalent to those found previously for $(\mu\text{-H})_2Ru_3(\mu_3\text{-}\eta^2\text{-}CHC(O)OCH_3)(CO)_9$ [2]. H(23) occupies a bridging "axial" site *trans* to C(22)–O(22) and C(32)–O(32) and H(13) occupies a bridging equatorial position in the Ru_3 plane *trans* to both C(11)–O(11) and C(33)–O(33).

Disregarding the direct Ru–Ru interactions between the hydride-bridged metal atoms (Ru(2)–Ru(3); Ru(1)–Ru(3)), each ruthenium atom has an octahedral coordination environment. The axial and equatorial ligands of Ru(1) are, respectively, perpendicular to, and coplanar with, the plane of the Ru_3 cluster. The ligands on Ru(2) and Ru(3) are rotated from this conformation to allow C(1) and H(23) to occupy sites in both coordination spheres. This is shown in Fig. 2 and is analogous to the situation in the parent complex.

$(\mu\text{-H})_2Ru_3(\mu_3\text{-}\eta^2\text{-}CHC(O)OCH_3)(CO)_9$ is much more labile than $(\mu\text{-H})_3Ru_3(\mu_3\text{-}CC(O)OCH_3)(CO)_9$, $(\mu\text{-H})_3Ru_3(\mu_3\text{-}COCH_3)(CO)_9$ [15], $(\mu\text{-H})Ru_3(\mu\text{-COMe})(CO)_{10}$ [16], or $Ru_3(CO)_{12}$ [17], all of which undergo ligand substitution over periods of many hours to days at 25°C, but is comparable in lability to $(\mu\text{-H})Ru_3(\mu\text{-CO})(CO)_{10}^-$ [18], and $Ru_3(CO)_{11}(C(O)OCH_3)^-$ [19], both of which are labilized by stabilization of the transition states for CO dissociation through electron donation by coordinated ligands. The unusual reactivity for $(\mu\text{-H})_2Ru_3(\mu_3\text{-}\eta^2\text{-}CHC(O)OCH_3)(CO)_9$ suggests that the μ_3-η^2-$CHC(O)OCH_3$ ligand labilizes the

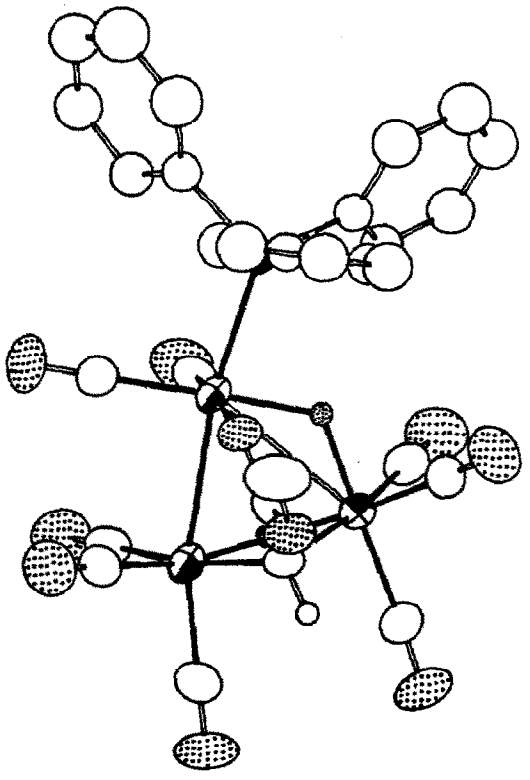

Fig. 2. View of the $(\mu\text{-H})_2Ru_3(\mu_3\text{-}\eta^2\text{-CHC(O)OCH}_3)(CO)_8(PPh_3)$ molecule, projected approximately (not exactly) onto the Ru_3 plane and showing the octahedral distribution of the ligands about each metal atom.

cluster to ligand substitution. Although we cannot rule out the possibility that the product is determined by thermodynamics rather than kinetics, the site of PPh_3 substitution suggests that the site for CO dissociation is the ruthenium atom to which the acyl oxygen is coordinated. The increased lability is most likely due to *cis* labilization induced by the oxygen donor ligand, a transition state stabilization effect [20]. An alternative possibility, dissociation of the coordinated acyl and attack by phosphine at the vacant coordination site, is highly unlikely, since addition of ligand in this case would form $(\mu\text{-H})_2Ru_3(\mu\text{-CHC(O)OCH}_3)(CO)_9L$, which, analogous to $(\mu\text{-H})_2Os_3(\mu\text{-CH}_2)(CO)_{10}$ [21], should undergo C–H elimination to form $(\mu\text{-H})Ru_3(CH_2C(O)OCH_3)(CO)_9L$; the stable analog $(\mu\text{-H})Os_3(CH_2C(O)OCH_3)(CO)_{10}$ [22] has been previously characterized, and, rather than undergoing ligand substitution in the presence of phosphine ligands, this cluster rapidly eliminates methyl acetate. Other instances of labilization of clusters by oxygen donors have been reported previously. For example- $(\mu\text{-H})Ru_3(\mu\text{-O=CR})(CO)_{10}^-$ undergoes rapid substitution on that ruthenium atom to which the acyl is O-coordinated [23]. Quantitative evaluations of *cis* labilization induced by bridging ligands in cluster systems are in progress.

Acknowledgement

This work was supported by the National Science Foundation through Grant CHE85-20276 to J.B.K. The mass spectrometer used in this study was purchased in

part with funds provided by the National Science Foundation (CHE-8613066). Special thanks go to Professor Bruce M. Foxman of Brandeis University for providing a copy of his IBM PC version of ORTEP-II [24].

References

1 Part XIII. M.R. Churchill, J.W. Ziller, D.M. Dalton, and J.B. Keister, Organometallics, 6 (1987) 806.
2 Part XII. M.R. Churchill, T.S. Janik, T.P. Duggan, and J.B. Keister, Organometallics, 6 (1987) 799.
3 Part XI. M.R. Churchill, T.P. Duggan, J.B. Keister, and J.W. Ziller, Acta Cryst. Section C, C43 (1987) 203.
4 Part X. M.R. Churchill, J.W. Ziller, and J.B. Keister, J. Organomet. Chem., 297 (1985) 93.
5 T.P. Duggan, M.J. Muscatella, D.J. Barnett, and J.B. Keister, J. Am. Chem. Soc., 108 (1986) 6076.
6 J.B. Keister and T.L. Horling, Inorg. Chem., 19 (1980) 2304.
7 M.R. Churchill, R.A. Lashewycz, and F.J. Rotella, Inorg. Chem., 16 (1977) 265.
8 Syntex XTL Operations Manual, 2nd ed., Syntex Analytical Instruments Inc., Cupertino, CA, 1976.
9 M.R. Churchill, Inorg. Chem., 12 (1973) 1213.
10 International Tables for X-Ray Crystallography; Kynoch: Birmingham, England, 1974, Vol. IV: (a) pp. 99–101 (b) pp. 149–150.
11 R_F (%) $= 100\Sigma||F_o| - |F_c||/\Sigma|F_o|$; R_{wF} (%) $= 100[\Sigma w(|F_o| - |F_c|)^2/\Sigma w|F_o|^2]^{1/2}$; $GOF = [\Sigma w(|F_o| - |F_c|)^2/(NO - NV)]^{1/2}$, where NO = number observations and NV = number of variables.
12 M.I.Bruce, T.W. Hambley, B.K. Nicholson, and J. Snow, J. Organomet. Chem., 24 (1982) 83.
13 A.V. Coleman, D.F. Jones, P.H. Dixneuf, C. Brisson, J.J. Bonnet, and G. Lavigne, Inorg. Chem., 23 (1984) 952.
14 E.J. Forbes, N. Goodhand, D.L. Jones, and T.A. Hamor, J. Organomet. Chem., 182 (1979) 143.
15 Z. Abdul Rahman, L.R. Beanan, L.M. Bavaro, S.P. Modi, J.B. Keister, and M.R. Churchill, J. Organomet. Chem., 263 (1984) 75.
16 D.M. Dalton, D.J. Barnett, T.P. Duggan, J.B. Keister, P.T. Malik, S.P. Modi, M.R. Shaffer, and S.A. Smesko, Organometallics, 4 (1985) 1854.
17 A.J. Poe and M.V. Twigg, J. Chem. Soc., Dalton Trans., (1974) 1860.
18 D.J. Taube and P.C. Ford, Organometallics, 5 (1986) 99.
19 M. Anstock, D. Taube, D.C. Gross, and P.C. Ford, J. Am. Chem. Soc., 106 (1984) 3696.
20 J.D. Atwood and T.L. Brown, J. Am. Chem. Soc., 98 (1976) 3155.
21 R.B. Calvert and J.R. Shapley, J. Am. Chem. Soc., 99 (1977) 5225.
22 J.B. Keister and J.R. Shapley, J. Am. Chem. Soc., 98 (1976) 1056.
23 C.E. Kampe and H.D. Kaesz, Inorg. Chem., 23 (1984) 4646.
24 C.K. Johnson, "ORTEP-II": A FORTRAN Thermal-Ellipsoid Plot Program for Crystal Structure Illustrations", Oak Ridge National Laboratory, Oak Ridge, TN (1976). IBM PC version by B.M. Foxman, Brandeis University, Waltham, MA (1987).